

262

NRL Report 8141

# Frequency-Agile Radar Signal Processing

W. M. WATERS and G. J. LINDE

*Search Radar Branch  
Radar Division*

November 15, 1977



**NAVAL RESEARCH LABORATORY**  
**Washington, D.C.**

Approved for public release; distribution unlimited.

REPORT DOCUMENTATION PAGE		READ INSTRUCTIONS BEFORE COMPLETING FORM
1. REPORT NUMBER NRL Report 8141	2. GOVT ACCESSION NO.	3. RECIPIENT'S CATALOG NUMBER
4. TITLE (and Subtitle) FREQUENCY-AGILE RADAR SIGNAL PROCESSING	5. TYPE OF REPORT & PERIOD COVERED Interim report on a continuing NRL Problem.	
	6. PERFORMING ORG. REPORT NUMBER	
7. AUTHOR(s) W. M. Waters and G. J. Linde	8. CONTRACT OR GRANT NUMBER(s)	
9. PERFORMING ORGANIZATION NAME AND ADDRESS Naval Research Laboratory Washington, D.C. 20375	10. PROGRAM ELEMENT, PROJECT, TASK AREA & WORK UNIT NUMBERS NRL Problem R02-92.101 ZF 12-151-001, 62712N	
11. CONTROLLING OFFICE NAME AND ADDRESS Naval Research Laboratory Washington, D.C. 20375	12. REPORT DATE November 15, 1977	
	13. NUMBER OF PAGES 20	
14. MONITORING AGENCY NAME & ADDRESS (if different from Controlling Office)	15. SECURITY CLASS. (of this report) UNCLASSIFIED	
	15a. DECLASSIFICATION/DOWNGRADING SCHEDULE	
16. DISTRIBUTION STATEMENT (of this Report) Approved for public release; distribution unlimited.		
17. DISTRIBUTION STATEMENT (of the abstract entered in Block 20, if different from Report)		
18. SUPPLEMENTARY NOTES		
19. KEY WORDS (Continue on reverse side if necessary and identify by block number) Detection Radar		
20. ABSTRACT (Continue on reverse side if necessary and identify by block number) Modern radars may incorporate pulse-to-pulse carrier frequency modulation to increase probability of detection, to reduce vulnerability to jamming, and to reduce probability of interception. However, if coherent processing is used for clutter rejection, the frequency of $N$ consecutive pulses must be held constant for $N$ -pulse clutter cancellation or doppler filtering. If $M$ pulses are transmitted during the time the antenna illuminates a target, there are $M/N$ coherently integrated echoes available for noncoherent integration in the computer or the operator's display		

(Continued)

20. Abstract (Continued)

to further improve the signal-to-noise ratio (SNR). In this report, analytical and simulation methods are employed to determine the balance between coherent and noncoherent integration that yields the greatest SNR improvement. Attention is focused upon three models which include FFT doppler filtering and different systems of combining and noncoherently integrating doppler filtered signals. Curves of detectable SNR as a function of  $M$  and  $N$  are presented for all three models.

## CONTENTS

INTRODUCTION .....	1
PROBLEM DEFINITION .....	1
PROCESSOR MODELS .....	2
Constant-Velocity Target Detector .....	3
Reference Processor .....	3
Peak Filter Output Integrator .....	3
DETECTABLE SNR FOR REFERENCE PROCESSOR .....	4
DETECTABLE SNR FOR PEAK FILTER OUTPUT INTEGRATOR .....	5
SIMULATION OF PEAK SELECTION PROCESSOR .....	7
CONCLUSIONS AND RECOMMENDATIONS .....	8
REFERENCES .....	11
APPENDIX A – Collapsing Loss Associated with Peak Output Selection and Integration .....	12
APPENDIX B – Signal-to-Noise Ratio Calculations .....	15
APPENDIX C – Collapsing Ratio Calculation .....	17



# FREQUENCY-AGILE RADAR SIGNAL PROCESSING

## INTRODUCTION

Modern radars sometimes incorporate pulse-to-pulse changes in carrier frequency (a) for the sake of increasing detection probability, (b) to reduce vulnerability to jamming, and (c) to reduce probability of interception. However, coherent processing such as a coherent moving-target indicator (MTI) is often necessary to suppress clutter echoes, which means that during the period of time coherent processing takes place, the carrier frequency should be held constant. It is possible, in principle, to perform coherent integration of a train of frequency-hopped echoes. However, the response of such a system to small changes in range and doppler frequency causes problems beyond the scope of this report. Thus, we consider a frequency-agile radar that transmits groups of  $N$  identical pulses, where carrier frequency is fixed within a group (block) but is varied from block to block.

In this report we address the problem of choosing the optimum value of  $N$  (the number of pulses in a constant-frequency block), assuming random frequency modulation from block to block. The total number of pulses  $M$  transmitted during the antenna beam dwell time is assumed to be fixed. The method explored here shows that a substantial improvement in receiver sensitivity results from an optimum choice of  $N$ , especially for large values of  $M$ .

Fundamental detection theory is reviewed in the next section and is subsequently applied to three receiver models, which are defined and analyzed. The appendixes provide needed detail to justify the method of calculating the performance of the receiver models.

## PROBLEM DEFINITION

Here we consider the problem of selecting optimum processing for a sequence of  $M$  radar echoes, which are divided into  $M/N$  blocks of  $N$  pulses per block. The carrier frequency  $f_n$ , (see Fig. 1) is assumed constant within a block; random changes in carrier frequency are assumed from block to block.  $M$  and  $N$  may take any integer value. An optimum processor is defined as one that minimizes the input signal-to-noise power ratio  $\mathcal{R}$  required for given probabilities of detection  $P_d$  and false alarm  $P_{fa}$ . If no further constraints are added, the optimum processor will be the well-known matched filter [1]. Since the waveform  $s(t)$  is known exactly (except for time of arrival), a linear filter, having an impulse response  $h(t) = \alpha s(-t + T_0)$ , would maximize the signal-to-noise ratio at its output and, hence, minimize detectable power,  $S$  (the constant,  $T_0 \geq$  pulse width, and  $S$  is sometimes termed receiver sensitivity).

At present, difficulties in implementation prevent coherent integration of frequency-agile echoes. Such a processor is known to have been implemented in software [2,3], but not, to the

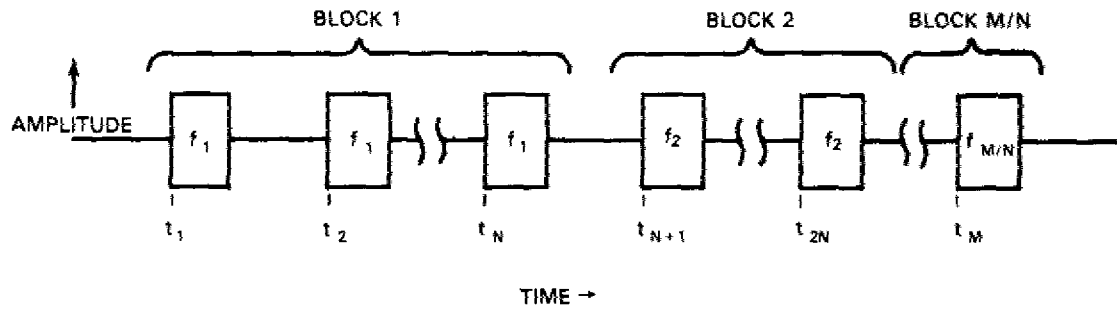


Fig. 1 — Block-to-block frequency-agile radar signal ( $f_n$  = carrier frequency)

best of our knowledge, in hardware. Hence, we consider coherent integration of each block of  $N$  pulses and noncoherent integration of  $M/N$  blocks. We wish to find a specific value of  $N$  which minimizes the input signal-to-noise ratio  $\mathcal{R}$  required for detection.

**PROCESSOR MODELS**

Figures 2a and 2b represent examples of the processors examined in this report. The processor of Fig. 2a is optimum under the above constraints, whereas the second processor (Fig. 2b) has the advantage of simplicity since only one output channel is required.

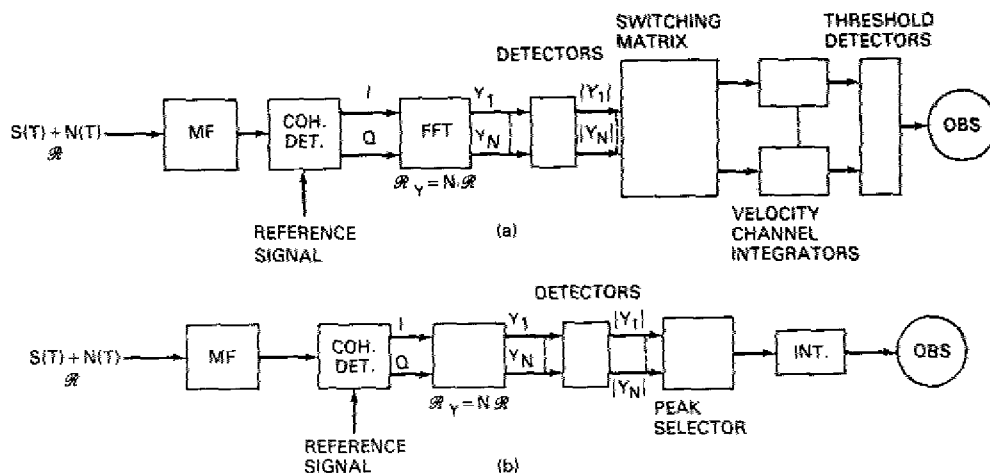


Fig. 2 — Block-to-block radar signal processing systems

A filter matched to a single doppler-shifted block of  $N$  pulses is identified by an impulse response matching the rectangular block of  $N$  pulses (Fig. 1). Since the doppler frequency is unknown, it is necessary to provide multiple filters to span the interval between doppler ambiguities. This leads to the incorporation of the well-known fast Fourier transform (FFT) as illustrated in Fig. 2; both processors are identical up through  $N$  magnitude detectors operating on  $N$  outputs from the  $N$ -point FFT. It is assumed that the filter block, labeled MF, is matched to the waveform of each pulse.

Detection theory [1,4] defines a maximum-likelihood detector for the case of a signal having one unknown parameter to be a bank of matched filters, which span the range of uncertainty (in this case doppler frequency), followed by threshold detectors operating on the filter output magnitudes. From this point of view (maximum-likelihood detection), an  $N$ -point FFT processor is optimum for detecting a target on the basis of a single block of pulses. We therefore incorporate, in the models of interest (Fig. 2), optimum  $N$ -pulse coherent processing.

### Constant-Velocity Target Detector

It can be argued that the processor of Fig. 2a is optimum for the signal specified in Fig. 1. An echo from a target of velocity  $v$  will be integrated in doppler filters identified by the relation  $f_{di} = 2f_i v/c$ , where  $f_{di}$  is the doppler frequency corresponding to the carrier frequency  $f_i$  of the  $i$ th block. Since the echo will appear in different doppler channels as  $f_i$  changes, a switching matrix is required to deliver all  $M/N$  coherently integrated blocks to the appropriate "video" integrator corresponding to target velocity  $v$ . It is noted that  $\Delta V/\Delta v$  velocity channels are required, where  $\Delta V$  is the range of target velocities and  $\Delta v = c/2NT_i f_i = \lambda/2NT_i$  is the mean velocity resolution of the FFT doppler channels.

Although we do not prove optimality, this processor integrates all echo energy over an  $M$ -pulse dwell time of the antenna beam on a target prior to combining with noise-only channels. Thus, this processor is expected to be more efficient\* than that of Fig. 2b, which combines doppler channels prior to video integration in the peak selector. The integrated outputs form the basis of an estimate of target velocity; i.e., all  $M/N$  outputs ( $|y_i|$ ) due to a target of velocity  $v$  will be connected via the switching matrix to the corresponding velocity channel integrator, say  $v_j$ . Hence, the threshold detectors, set to select the largest response, will most probably select the one containing the target signal. In this sense, the processor of Fig. 2a may be referred to as a velocity estimator, where  $v_j$  is an estimate of target velocity  $v$ .

### Reference Processor

Here we define a reference processor which is identical to that of Fig. 2a except that only one velocity channel (hence, one video integrator) is required since we assume that target velocity is known. The effect of this assumption is to avoid the need to correct calculated SNR values for doppler uncertainty. If the doppler frequency is unknown, the threshold values must be increased, as  $\Delta V/\Delta v$  increases, to maintain a constant false alarm rate.

### Peak Filter Output Integrator

The advantage of processing block-to-block agile signals, using the system of Fig. 2b rather than that of Fig. 2a, is obvious; no switching matrix and just one integrator are required. On the other hand, a disadvantage stems from the fact that no doppler information is available from the peak output integrator. When samples of noise only are added to samples containing signal plus noise, the signal becomes more difficult to discern from noise, and the increase in signal power required to maintain a given detection reliability ( $P_d$  and  $P_{fa}$ ) is referred to as collapsing loss. However, as will be shown later, the performance for Fig. 2b is only slightly worse than that for the reference processor defined above.

\*This term is used to express efficacy of signal-to-noise ratio improvement; efficiency in mathematical statistics takes on a different meaning not intended here.

## DETECTABLE SNR FOR REFERENCE PROCESSOR

We now develop, for the above-defined reference processor, an expression for  $\mathcal{R}$ , the input SNR required for specified detection and false alarm probabilities. To obtain this expression, we assume that SNR is improved linearly with  $N$  in the coherent integrator (FFT), and we make use of the standard curves of  $\mathcal{R}_y$  needed (for different combinations of  $P_d$  and  $P_{fa}$ ) at the input to the magnitude detector as functions of  $I = M/N$ , the number of noncoherent integrations. The calculation of  $\mathcal{R}_y$  ( $P_d = 0.9$ ,  $P_{fa} = 0.7 \times 10^{-10}$ ) is plotted in Fig. 3, based upon the five statistical models defined by Swerling [5] for targets with fluctuating cross section. Probably, the most frequently used is Case I, which corresponds to Rayleigh scan-to-scan fluctuations (all  $I$  pulses correlated). Cases I and III differ only in the statistical distributions assumed. The results in Fig. 3 clearly illustrate the greater penalty inflicted by the Case I scan-to-scan fluctuations as compared with the Case II pulse-to-pulse fluctuations for large values of  $I$ , the number of integrated pulses. Note that for  $I = 750$ , Case II noncoherent integration (NCI) is more efficient than Case I NCI by about 8 dB.

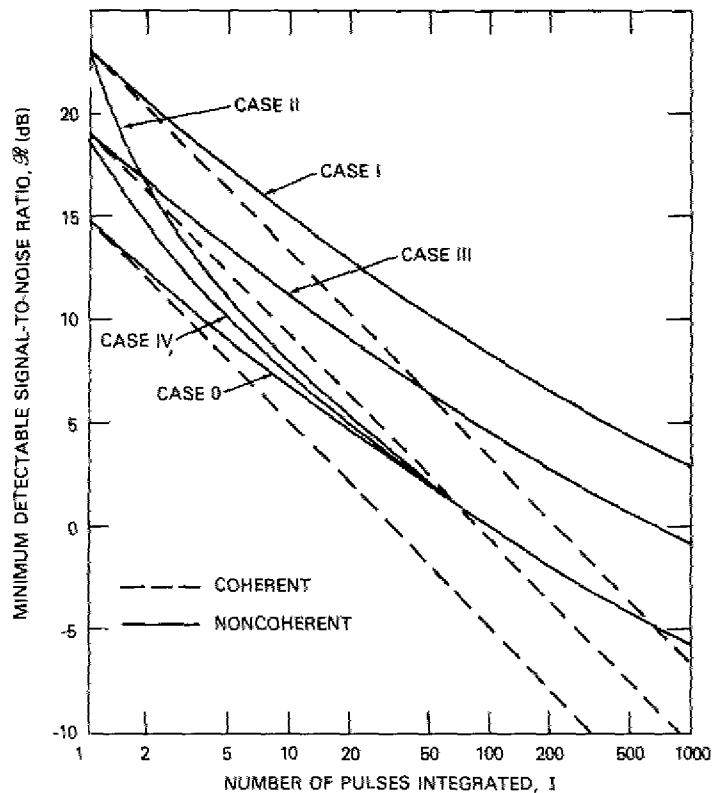


Fig. 3 — Comparison of coherent and noncoherent integration of radar returns from Swerling-model targets (for  $P_d = 0.9$ ,  $P_{fa} = 0.7 \times 10^{-10}$ ) (after Rivers, SEMCOR Rept. SD-75213-1)

The curves of Fig. 4 were developed from Swerling Case II curves (frequency agility block-to-block), making use of the following procedure and definitions. The detectable SNR at the input,  $\mathcal{R}$ , is improved by coherent integration so that  $\mathcal{R}_y = N\mathcal{R}$ , neglecting losses; hence, a value of  $\mathcal{R}$  may be found from Eq. (1):

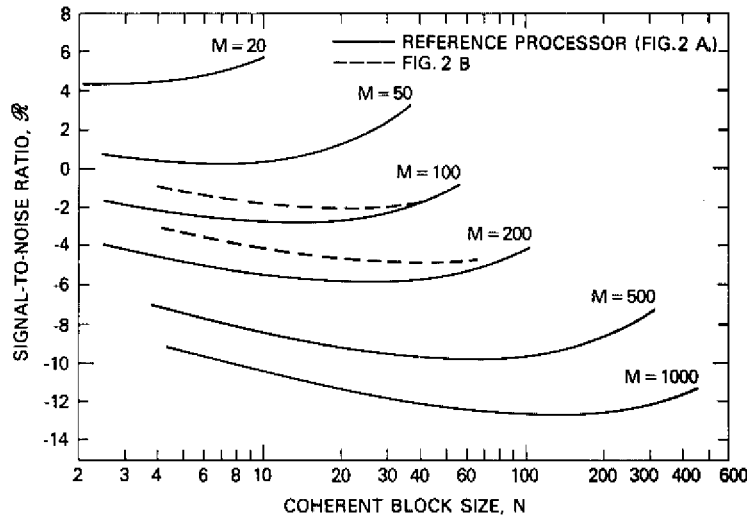


Fig. 4 — Required signal-to-noise ratio (for  $P_d = 0.9$ ,  $P_{fa} = 0.7 \times 10^{-10}$ ) vs  $N$  for fixed values of  $M$  (pulses/dwelltime)

$$\mathcal{R} = (1/N) \mathcal{R}_y (M/N). \tag{1}$$

For example, note that for Case II (Fig. 3),  $\mathcal{R}_y (100/10)/10 \approx 8 - 10 = -2 \text{ dB} = \mathcal{R}$ .

### DETECTABLE SNR FOR PEAK FILTER OUTPUT INTEGRATOR

The curves of Figs. 4 and 5, corresponding to the processor of Fig. 2b, required a more complex calculation because of the necessity of accounting for the collapsing loss encountered when noise-only channels are combined with a channel containing both signal and noise. Thus, we make use of the fact that a portion of this processor has been analyzed for M-ary communications [4]. In this case, the block diagram up through the peak selector is identical to the optimum detector for a communications signal consisting of any one of  $N$  orthogonal signal waveforms. The probability of error (i.e., the probability that the output of at least one noise-only channel will exceed the output of the channel containing the signal) is computed using the relation of Eq. (2), which is further illustrated by the graph of Fig. 6;

$$P_r(\epsilon) = 1 - \int_{-\infty}^{+\infty} dx \frac{1}{\sqrt{2\pi}} \exp\left\{-\frac{[x - (2E/N_0)^{1/2}]^2}{2}\right\} \cdot \left[ \int_{-\infty}^x \frac{1}{\sqrt{2\pi}} \exp(-y^2/2) dy \right]^{N-1}, \tag{2}$$

where  $E$  and  $N_0$  are signal energy and noise power spectral density, respectively.

Returning to Figs. 3 and 4, note that the minima exhibited by the curves of Fig. 4 occur because of the change in slope of the Case II curve (solid line) in Fig. 3, as  $I = M/N$  changes from small to large values. Its slope exceeds that of the corresponding coherent integration curve (dashed line) for small  $I$  becoming smaller for large  $I$ . As  $N$  approaches  $M$  (Fig. 4),  $I$  decreases to small values causing the value of  $\mathcal{R}_y$  (Fig. 3) to rise sharply, overcoming the decrease due to greater coherent processing.

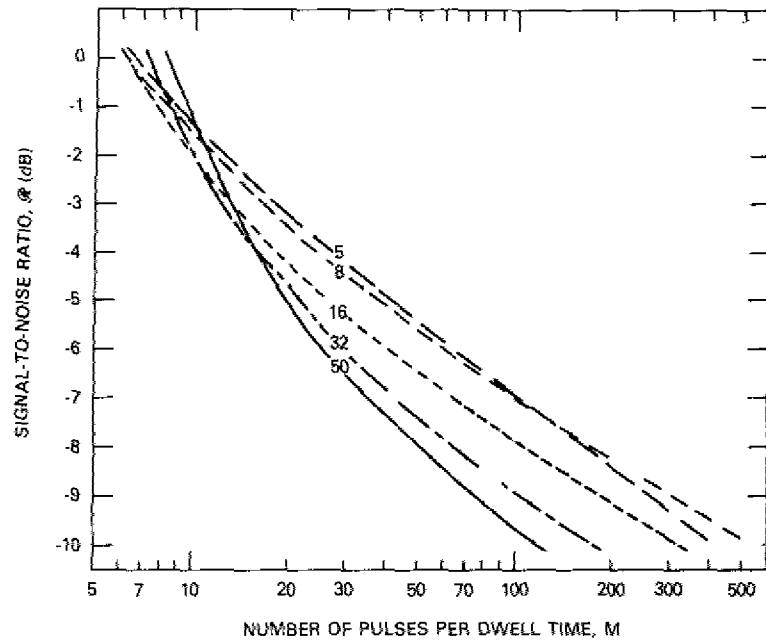


Fig. 5 — Required signal-to-noise ratio (for  $P_d = 0.9$ ,  $P_{fa} = 0.7 \times 10^{-10}$ ) vs.  $M$  for fixed values of  $N$  (coherent block size)

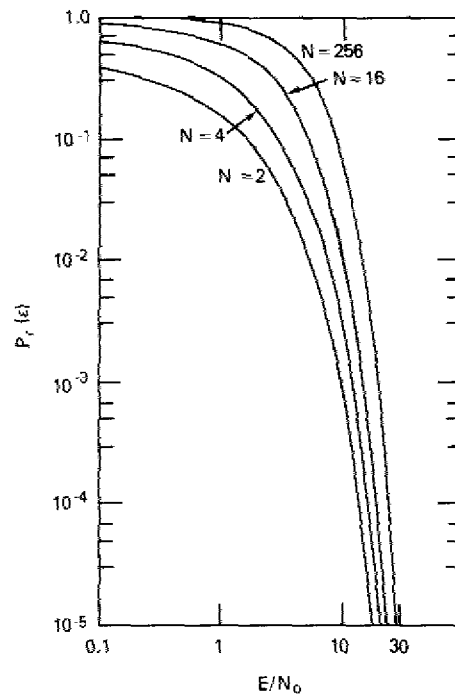


Fig. 6 — Error probability:  $N$  orthogonal signals

Hence, if we consider a sequence of  $I$  output samples from the peak selector, on the average,  $P_r I$  samples will be due to noise only; clearly  $(1 - P_r)I$  will be due to signal plus noise. Collapsing loss is well known [6] to be a function of the collapsing ratio  $\rho_c$ , where, if  $m$  is the number of noise-only samples and  $n$  is the number of signal-plus-noise samples, then

$$\rho_c = \frac{m+n}{n} = \frac{P_r I + (1 - P_r)I}{(1 - P_r)I} = \frac{1}{1 - P_r} \quad (3)$$

Although Marcum [7] calculated collapsing loss  $L_c$  as a function of this ratio  $\rho_c$ , his curves (reprinted by Berkowitz [8]), were computed for the case of a nonfluctuating target. The approximation ( $L_c \approx 1 - P_r$ ), as discussed in Appendix A, is therefore used below to derive Eq. (4).

Since  $L_c$  is a function of  $P_r$ , which is a function of  $\mathcal{R}$  and  $N$ , we are led to the following equation which must be solved by successive approximations:

$$N\mathcal{R} = \mathcal{R}_y (M/N) / L_c = \frac{\mathcal{R}_y (M/N)}{1 - P_r(\mathcal{R}, N)} \quad (4)$$

Equation (4) is obtained from the definition of, and approximation for, collapsing loss (see Appendix A) and the relationship  $\mathcal{R}_y = N\mathcal{R}$  for coherent integration. Note that  $L_c$  is defined to be a number less than one.

### SIMULATION OF PEAK SELECTION PROCESSOR

A simulation was implemented to compute the detection performance of a processor using peak selection of doppler channels. For comparison, the simulation was also run for a processor using only a single doppler channel. Figure 7 is a diagram of the simulation showing the processors and the signal and noise generators.

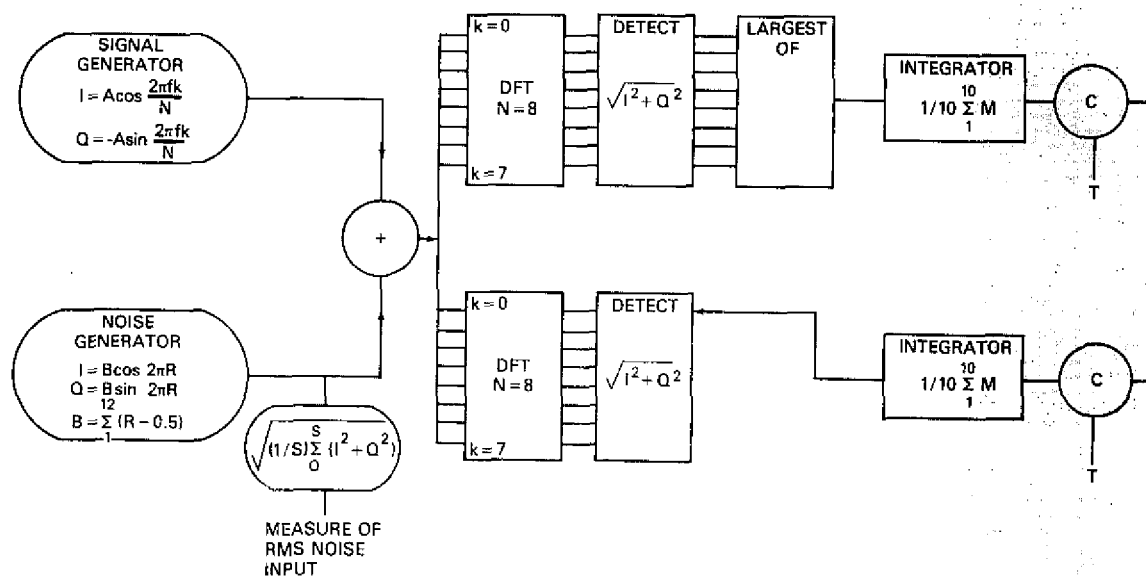


Fig. 7 - Simulation of "largest of" detector and single doppler channel detector

The processor of interest consists of a doppler filter bank, implemented with an eight-point discrete Fourier transform (DFT). Eight input samples compose a coherent processing interval (CPI) and produce eight doppler outputs. The outputs are detected, the one with the largest amplitude is selected, and the outputs from 10 CPIs are summed in a noncoherent integrator. Finally, the output of the integrator is compared to a fixed threshold and the detection decision is made. The detection decision is based on a total dwell time of  $M = 80$  samples. The second processor is then implemented as a reference. This processor, identical except that a single doppler output is used, represents a case where the target doppler is known and no collapsing loss is suffered.

The inputs to both processors are identical and consists of in-phase and quadrature ( $I$  and  $Q$ ) components of signal plus noise. The signal components are

$$I_s = A \cos \frac{2\pi f k}{N} \quad (5a)$$

and

$$Q_s = A \sin \frac{2\pi f k}{N}, \quad (5b)$$

where  $f$  is the doppler frequency,  $k$  the doppler filter number, and  $N$  the number of points in the DFT. The additive noise has a uniform phase distribution and an approximately Gaussian amplitude distribution given by

$$I_N = B \cos 2\pi R, \quad (6a)$$

$$Q_N = B \sin 2\pi R, \quad (6b)$$

and

$$B = \sum_1^{12} (R - 0.5), \quad (6c)$$

where  $R$  is a uniformly distributed random number between 0.0 and 1.0.

The first step in the simulation is to determine the threshold setting  $T$  for various false alarm rates. The results shown in Fig. 8 were obtained by setting the input signal to zero and measuring the probability of false alarm as a function of the threshold setting. Now, we can use threshold settings at a desired  $P_{fa}$  and measure  $P_d$  by running the simulation with various values of signal amplitude.

The results of the simulation of both processors are shown in Fig. 9, where the input SNR is plotted as a function of  $P_d$  for various  $P_{fa}$ . For a  $P_d = 0.9$  and  $P_{fa} = 10^{-3}$ , the processor selecting the largest filter output requires 2.3 dB higher SNR than the reference processor. For greater  $P_d$  and smaller  $P_{fa}$ , the performance of the "largest of" processor approaches that of the single filter case.

## CONCLUSIONS AND RECOMMENDATIONS

We have shown that the choice of block size in a block-to-block frequency-agile radar is important if maximum receiver sensitivity is to be realized. The curves of Fig. 4 exhibit distinct minima in signal-to-noise ratio required for reliable detection, the locations of which depend upon the total number of pulses available for coherent and noncoherent processing.

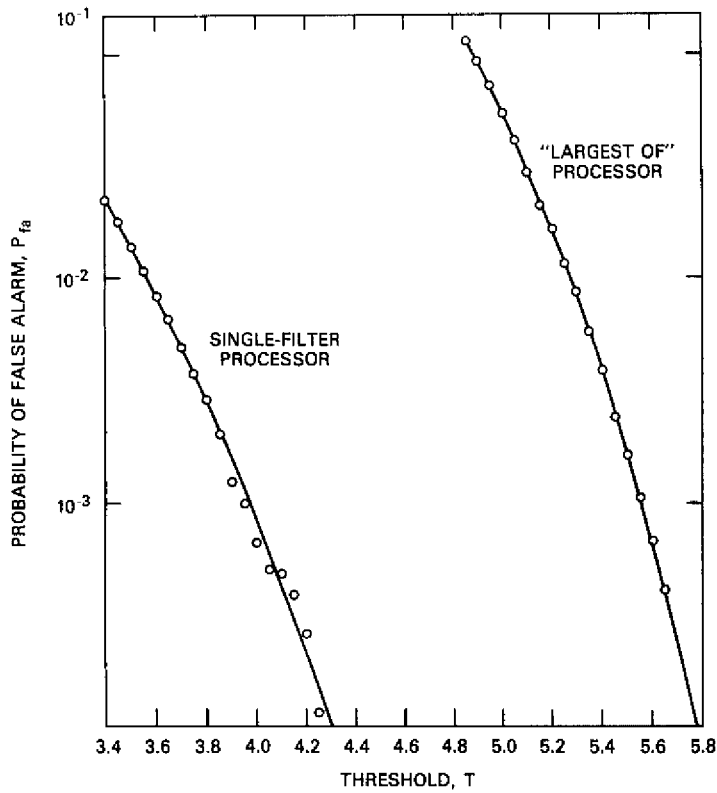


Fig. 8 — Probability of false alarm as a function of threshold setting

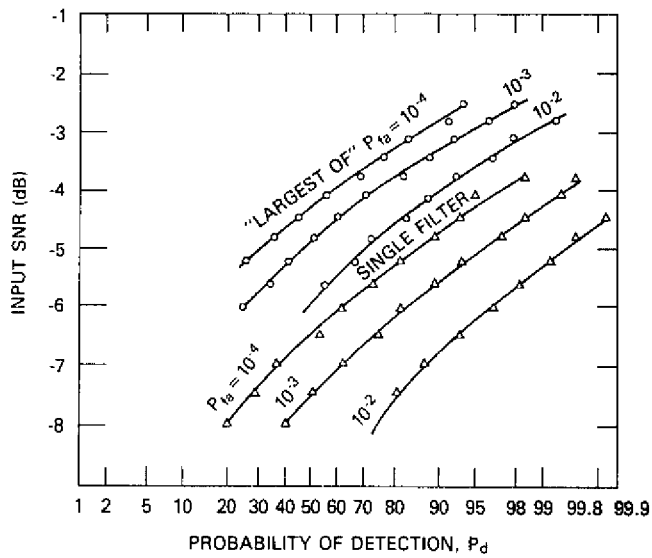


Fig. 9 — Signal-to-noise ratio vs  $P_d$  and  $P_{fa}$  from computer simulations

These data correspond to a reference case in which it is presumed that the doppler frequency of the target is known, so that collapsing loss is zero. The collapsing loss corresponding to the velocity-estimator processing (Fig. 2a) is easily determined from the reference case (to a good approximation) by computing the number of doppler resolution cells required to span the range of target velocities. If this number is greater than  $N$ , then the collapsing loss is equal to the SNR increase needed to reduce  $P_{fa}$  by the factor  $N$ . Here, collapsing loss arises from the fact that more than one channel may contribute a false alarm, requiring an increase in threshold and SNR to maintain a desired false alarm rate.

Figure 4 also contains data corresponding to peak select/integrate processing (Fig. 2b) in which multiple doppler channels are combined by selecting only the largest output for subsequent video integration. Table 1 compares the three processors for two values of total dwell time,  $M = 100$  and  $M = 200$ , where in each case the optimum  $N$  was selected.

Table 1 — Comparison of Processor Performance  
( $P_d = 0.9$ ,  $P_{fa} = 10^{-8}$ )

Processor	$M$	$N_{opt}$	SNR (dB)	$L_c$ (dB)
Reference	100	17	-3.6	0
	200	33	-6.8	0
Velocity Estimator (Fig. 2a)	100	17	-2.75	0.85
	200	33	-5.15	1.65
Peak Select/Integrate (Fig. 2b)	100	20	-2.1	1.5
	200	50	-5.1	1.7

It should be noted that the SNR penalty for using the simpler system involving just one integrator is less than 1 dB for  $M = 100$ , and less than 0.1 dB for  $M = 200$ . However, we must consider the effect of the approximation used in calculating performance of the latter system. Basically, the approximation involves two assumptions discussed in greater detail in Appendix A:

1. We assumed  $\mathcal{R}_z \sim \mathcal{R}_y$  in deriving Eq. (4) used to compute SNR for the peak select/integrate system.

2. The effect of the peak selector on signal and noise distributions was ignored; i.e.,  $P_d$  and  $P_{fa}$  were assumed to depend only on  $\mathcal{R}_0$ , the SNR at the threshold.

Table 2 compares the data calculated from Eqs. (1) and (4) with Monte Carlo simulations of the reference and the peak select/integrate processors. No approximations are involved in Eq. (1) except those used by Marcum, and the signal in the development of Table 2 is nonfluctuating. The results clearly indicate that the simulation and the calculation for the reference processor agree within 0.2 dB; the simulation for the peak selector is higher by 0.5 dB than the computed result involving  $L_c = 1 - P_r$ , and 1.1 dB for the case involving  $L_c = \sqrt{1 - P_r}$ . These collapsing loss expressions, described in Appendix A, hold for large and small SNR, respectively. It might be inferred from Table 2 that the effect of the second assumption (mentioned above) is to yield optimistic results; hence,  $L_c = 1 - P_r$  provides a

more accurate estimate of SNR. This would tend to agree with the expected influence of the peak selector upon the noise statistics; i.e., it is reasonable to expect the distribution change to increase  $P_{fa}$ . It has been suggested that  $L_c$  depends more heavily on  $N$  than on  $M$ , the total number of integrated pulses [9].

Table 2 — Comparison of Performance Estimates Obtained from Eqs. (1) and (4) and Corresponding Monte Carlo Simulation\*

Processor	Method	SNR (dB)
Reference	Eq. (1)	-4.9
Reference	Simulation	-4.7
Peak Select/Integrate	Eq. (4) ( $L_c = 1 - P_r$ )	-3.3
Peak Select/Integrate	Eq. (4) ( $L_c = \sqrt{1 - P_r}$ )	-3.9
Peak Select/Integrate	Simulation	-2.8

\* $P_d = 0.9$ ,  $P_{fa} = 10^{-4}$ ,  $M = 80$ ,  $N = 8$

In conclusion, it should also be noted that the processor of Fig. 2a provides an estimate of target doppler as well as nearly optimum sensitivity. Further attention should be given to this technique. For example, a measure of reliability of velocity data for targets of various speeds and accelerations could be defined and tested. Although the utility of frequency-agile systems depends on the range of frequencies available and interference with other users of microwave bands, doppler ambiguities are reduced and blind speeds are eliminated by this technique, so that an estimate of radial velocity is available on each scan of the antenna. Velocity data should tend to reduce track-while-scan errors and the hand-off delay to weapons systems.

#### REFERENCES

1. G.L. Turin, "An Introduction to Matched Filters," *IRE Trans. IT-6*, 311-329 (Jun. 1960).
2. P.N. Marinos and W.M. Waters, "A Proposed Coherent Integration Scheme for Use in Frequency-Agile Radar Systems," IEEE Div. III Conf., (Apr. 1974).
3. K. Ruttenberg and L. Chanzit, "High Range Resolution by Means of Pulse-to-Pulse Frequency Shifting," EASCON (Electronics and Aerospace Systems Convention) 1968 Record, pp. 47-51.
4. H.L. Van Trees, *Detection, Estimation, and Modulation Theory*, John Wiley and Sons, Inc., New York, 1968.
5. P. Swerling, "Probability of Detection for Fluctuating Targets," Rand Corp. Research Memo RM-1217, Mar. 1954 (reprinted in *IRE Trans. IT-6*, 269-308 (Apr. 1960)).
6. F.E. Nathanson, *Radar Design Principles*, McGraw-Hill Book Co., 1969.
7. J.I. Marcum, "A Statistical Theory of Target Detection by Pulsed Radar," Rand Research Memo RM-754, 1 Dec. 1947 and RM-753, July 1948 (reprinted in *IRE Trans. IT-6* (No. 2), 59-267, 1960).
8. R.S. Berkowitz, *Modern Radar*, John Wiley and Sons, Inc., New York, 1965.
9. Dr. G.V. Trunk, Radar Division, Naval Research Laboratory, private communication.

## Appendix A

### COLLAPSING LOSS ASSOCIATED WITH PEAK OUTPUT SELECTION AND INTEGRATION

In this appendix, we are interested in finding the value of  $\mathcal{R}_y$  needed to provide the required detection reliability measured by  $P_d$  and  $P_{fa}$  (detection and false alarm probabilities) for the system illustrated in Fig. A1. Since  $N-1$  noise-only channels are combined with the channel containing the signal in a peak selector, the SNR delivered to the integrator is degraded; to compensate,  $\mathcal{R}_y$  must be increased by an amount defined here to be the collapsing loss  $L_c$ . The necessary increase in  $\mathcal{R}_y$  may be approximated by introducing the diagram of Fig. A2. Here,  $\mathcal{R}'_y$  is the SNR needed if all integrated pulses contain signal plus noise and we define collapsing loss as

$$L_c = \mathcal{R}'_y / \mathcal{R}_y. \quad (A1)$$

Note that the output SNR,  $\mathcal{R}_0$ , is the same for both diagrams (Figs. A1 and A2). Although it is known that, in general, equal detection reliabilities ( $P_d, P_{fa}$ ) will not be achieved by making  $\mathcal{R}_0$  the same in Figs. A1 and A2 because of the differing statistical distributions caused by the effect of the peak selector (Fig. A1), comparisons of data computed from the results of the following analysis indicate that this effect is small.

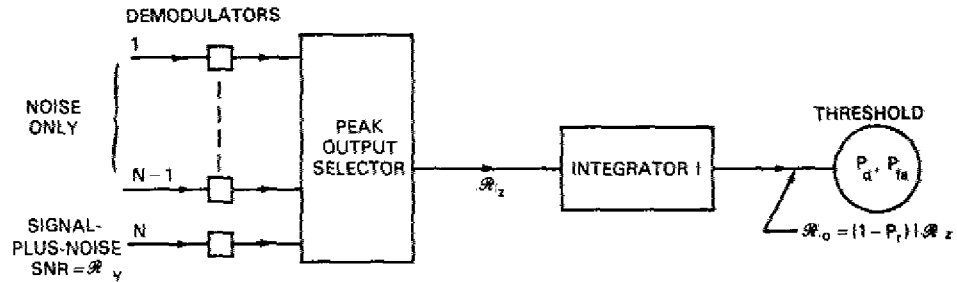
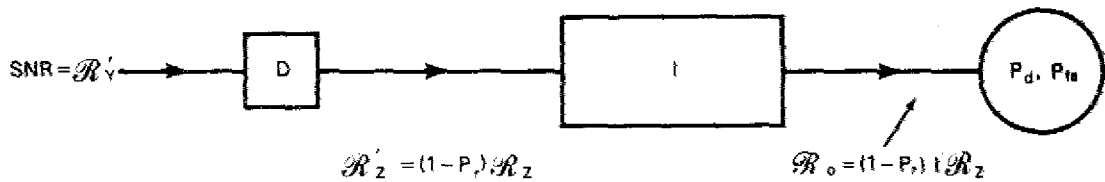


Fig. A1 — Noncoherent integration of peak-selected doppler filtered signals



(b)

Fig. A2 — Single channel model with equivalent output SNR

We assume that SNR improves linearly with  $I$ , because of video integration, so that, in Fig. A1,  $\mathcal{R}_0 = \sum_{i=1}^I \mathcal{R}_{zi}$ . A signal is assumed to be present in just one of the  $N$  doppler channels and SNR is assumed to be  $\mathcal{R}_y$ . Equal amounts of noise are assumed in all channels. On the average,  $P_r I$  integrated pulses are due to noise only (i.e.,  $\mathcal{R}_{zi} = 0$ ) where  $P_r$  is the so-called error probability described in the foregoing sections and in Appendix C. Hence, if  $\mathcal{R}_y$  is assumed constant for  $I$  pulses, then  $\mathcal{R}_{zi} = \mathcal{R}_z$  for the remaining  $(1 - P_r)I$  terms, and

$$\mathcal{R}_0 = \sum_{i=1}^{(1-P_r)I} \mathcal{R}_z = (1 - P_r)I \mathcal{R}_z. \quad (\text{A2})$$

In Fig. A2,  $\mathcal{R}'_z = \mathcal{R}_0/I = (1 - P_r)\mathcal{R}_z$ , since  $\mathcal{R}_0$  is the same (Eq. (A2)) as in Fig. A1 and  $\mathcal{R}_z$  is assumed to be constant.

Now, to evaluate  $L_c = \mathcal{R}'_y/\mathcal{R}_y$ , we introduce an expression connecting  $\mathcal{R}'_y$  with  $\mathcal{R}_y$ . Equation (A3), given by Davenport and Root,\* makes clear the nonlinear dependence of  $\mathcal{R}_z$  on  $\mathcal{R}_y$ . The same expression connects  $\mathcal{R}_z$  and  $\mathcal{R}_y$ .

$$\mathcal{R}_z = k_p \frac{\mathcal{R}_y^2}{1 + 2\mathcal{R}_y}, \quad (\text{A3})$$

where  $k_p = 1$  for a rectangular sine wave signal envelope. Equation (A3) holds for Gaussian noise, a square law detector, and where  $\mathcal{R}_z$  is defined as the ratio of output signal and noise-only powers. Although the equation for  $\mathcal{R}_z$  varies with assumptions regarding detector law and SNR definition, we are dealing here with a mechanism affected only slightly by the functional dependence of  $\mathcal{R}_z$  on  $\mathcal{R}_y$ . In the following paragraphs, this is demonstrated by comparing values of  $L_c$  obtained by calculations based upon two assumptions: (a)  $\mathcal{R}_z \sim \mathcal{R}_y$  and (b)  $\mathcal{R}_z$  as given by Eq. (A3).

Let  $\mathcal{R}_z = f(\mathcal{R}_y)$ , where an example of the function  $f$  is given in Eq. (A3). Note that the collapsing loss  $L_c$  may be expressed in terms of the inverse function  $f^{-1}$ . Since  $\mathcal{R}'_y = f^{-1}(\mathcal{R}'_z)$ , we may substitute this expression into Eq. (A1), and we have

$$L_c = \frac{f^{-1}(\mathcal{R}'_z)}{f^{-1}(\mathcal{R}_z)} = \frac{f^{-1}[(1 - P_r)\mathcal{R}_z]}{f^{-1}(\mathcal{R}_z)}, \quad (\text{A4})$$

where the right-hand side of Eq. (A4) makes use of the substitution  $\mathcal{R}'_z = (1 - P_r)\mathcal{R}_z$ , derived from Eq. (A2).

If we let  $\mathcal{R}_z \sim \mathcal{R}_y$ , then Eq. (A4) reduces to the form introduced in the text in Eq. (4); i.e.,  $L_c = 1 - P_r$ . If we require greater accuracy (especially for  $\mathcal{R}_y \ll 1/2$ ), we must use Eq. (A5) obtained from Eqs. (A2) and (A4).

$$L_c = \frac{\mathcal{R}_y (1 - P_r)}{1 + 2\mathcal{R}_y} \left[ 1 + \sqrt{\frac{1 + 2\mathcal{R}_y}{(1 - P_r)\mathcal{R}_y^2}} \right]. \quad (\text{A5})$$

\*W. B. Davenport, Jr. and W. L. Root, *An Introduction to the Theory of Random Signals and Noise*, McGraw-Hill, New York, 1958, p. 266.

In solving Eq. (A3) for  $\mathcal{R}_y$ , two roots result; the root leading to negative values of  $\mathcal{R}_y$  was discarded.

Equation (A5) is plotted in Fig. A3 for several values of  $P_r$ . Note that the approximation  $\sqrt{1 - P_r} \approx L_c$  holds for small values of  $\mathcal{R}_y \ll 1/2$  with  $L_c \approx 1 - P_r$  for  $\mathcal{R}_y \gg 1/2$ .

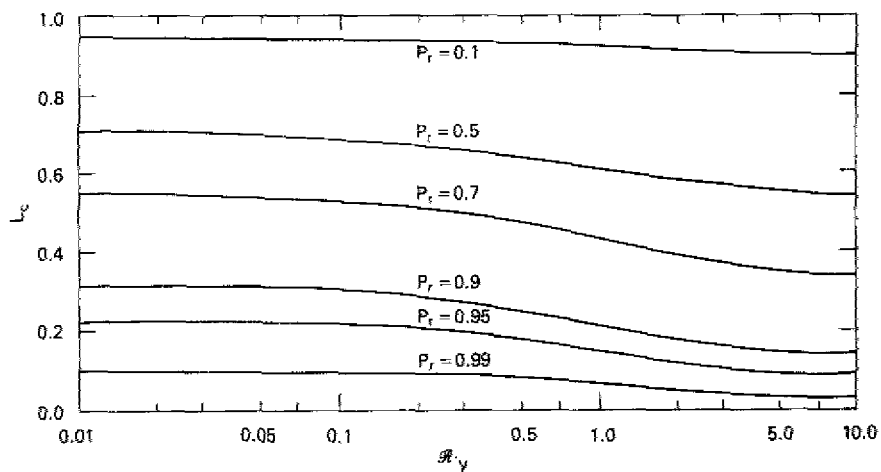


Fig. A3 — Collapsing loss (Eq. (A5)) vs. signal-to-noise ratio  $\mathcal{R}_y$  and error probability  $P_r$

**Appendix B**  
**SIGNAL-TO-NOISE RATIO CALCULATIONS**  
**FOR SWERLING CASE II**

Original works by Marcum\* and Swerling† have been discussed by many authors. A report by L. F. Fehner‡ includes calculations for the pulse-to-pulse fluctuation case, Swerling Case II (SW-2). All five of their statistical models are illustrated in the curves of Fig. B1. The purpose of this appendix is to present expressions for  $P_d$  and  $P_{fa}$  for SW-2.

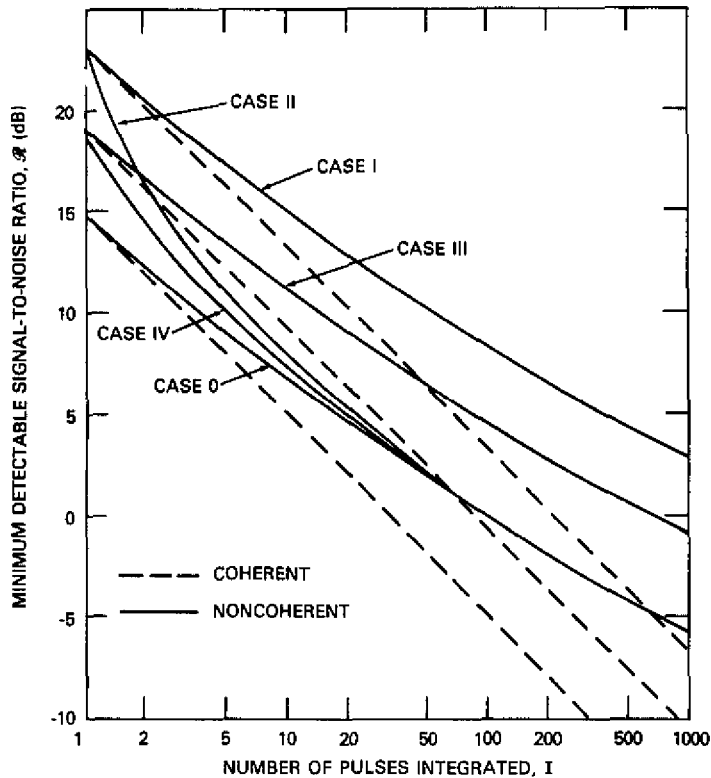


Fig. B1 — Comparison of coherent and noncoherent integration of radar returns from Swerling-model targets (for  $P_d = 0.9$ ,  $P_{fa} = 0.7 \times 10^{-10}$ ) (after Rivers, SEMCOR Rept. SD-75213-1)

\*J. I. Marcum, "A Statistical Theory of Target Detection by Pulsed Radar, Rand Research Memo RM-754, Dec. 1947, and RM-653, July 1948 (reprinted in *IRE Trans. IT-6*, (No. 2), 59-267 (1960).

†P. Swerling, "Probability of Detection for Fluctuating Targets," Rand Corp. Research Memo RM-1217, Mar. 1954 (reprinted in *IRE Trans. IT-6*, 269-308 (Apr. 1960).

‡L. F. Fehner, "Target Detection by a Pulsed Radar," Johns Hopkins Applied Physics Laboratory Report TG 451, Jul. 1962.

Equation (B1) expresses the probability of detection  $P_d$  and false alarm  $P_{fa}$  for SW-2 in terms of  $\mathcal{R}$  and the number of noncoherent integrations,  $I$ .

$$P_d = 1 - \int_0^{\frac{T}{I+\mathcal{R}}} \left\{ \frac{e^{-y} y^{I-1}}{(I-1)!} \right\} dy, \quad (\text{B1})$$

where  $P_{fa} = P_d$  when  $\mathcal{R} = 0$  and where the parameter  $T$  equals the detection threshold level normalized to the rms noise at the detector input.

Note that the SW-2 curve in Fig. B1 was obtained from Eq. (B1) with  $P_d = 0.9$  and  $T$  such that

$$P_{fa} = 0.7 \times 10^{-10} = 1 - \int_0^T \left\{ \frac{e^{-y} y^{I-1}}{I-1!} \right\} dy. \quad (\text{B2})$$

**Appendix C**  
**COLLAPSING RATIO CALCULATION**

Van Trees\* discusses "M-ary" detection of signals in additive, white Gaussian noise. The expression is presented in Eq. (C1) (also in Eq. (2) in the text) for error probability  $P_r(\epsilon)$ . This quantity, used in this report to compute the collapsing ratio  $\rho_c$  and collapsing loss  $L_c$ , is given as

$$P_r(\epsilon) = 1 - \int_{-\infty}^{+\infty} dx \frac{1}{\sqrt{2\pi}} \exp\left\{-\frac{[x - (2E/N_0)^{1/2}]^2}{2}\right\} \cdot \left[ \int_{-\infty}^x \frac{1}{\sqrt{2\pi}} \exp(-y^2/2) dy \right]^{N-1}. \quad (C1)$$

The double integral in Eq. (C1) has been evaluated extensively by Urbano.† Tables of values from his report were utilized in our analysis as follows:

Urbano's tabulated function  $P_\mu(a)$  is identical to the second term of (C1) if substitutions for  $N$  and  $a$  are made and if the variable of integration is changed appropriately. Thus,

$$P_\mu(a) = \frac{1}{\sqrt{2\pi}} \int_{-\infty}^{+\infty} e^{-z^2/2} \left[ \int_{-\infty}^{z+a} \frac{e^{-y^2/2}}{\sqrt{2\pi}} dy \right]^{\mu-1} dz. \quad (C2)$$

Letting  $z = x - a$  results in

$$P_N(a) = \frac{1}{\sqrt{2\pi}} \int_{-\infty}^{+\infty} e^{-\frac{[x-a]^2}{2}} \left[ \int_{-\infty}^x \frac{e^{-y^2/2}}{\sqrt{2\pi}} dy \right]^{N-1} dx. \quad (C3)$$

By inspection of (C1) and (C3), we may write,

$$P_r(\epsilon) = 1 - P_N(a) \quad (C4)$$

if we let  $a = \sqrt{2E/N_0}$ , where  $E$  is the energy in each input signal waveform and  $N_0$  is the input noise power density.

\*H. L. Van Trees, *Detection, Estimation, and Modulation Theory*, John Wiley and Sons, Inc., New York, 1968.

† R. H. Urbano, "Analysis and Tabulation of the M-Positions Experiment Integral and Related Error Function Integrals," AFRC Report TR-55-100, Apr. 1955.